Hideki Hasegawa ORCID iD: 0000-0002-6558-2297

Noriyo Nagata ORCID iD: 0000-0001-9147-1438

Gold nanoparticle-adjuvanted S protein induces a strong antigen-specific IgG response against severe acute respiratory syndrome-related coronavirus infection, but fails to induce protective antibodies and limit eosinophilic infiltration in lungs

Short title: A subunit vaccine against coronavirus

Subject sections: Vaccines and antiviral agents

Hanako Sekimukai[1, 2], Naoko Iwata-Yoshikawa[1], Shuetsu Fukushi[3], Hideki Tani[3#a], Michiyo Kataoka[1], Tadaki Suzuki[1], Hideki Hasegawa[1], Kenichi Niikura[4#b], Katsuhiko Arai[2], and Noriyo Nagata[1]*

[1] Department of Pathology, National Institute of Infectious Diseases, Musashimurayama, Tokyo, Japan

This article has been accepted for publication and undergone full peer review but has not been through the copyediting, typesetting, pagination and proofreading process, which may lead to differences between this version and the Version of Record. Please cite this article as doi: 10.1111/1348-0421.12754.

[2] Department of Tissue Physiology, Faculty of Agriculture, Tokyo University of Agriculture and Technology, Fuchu, Tokyo, Japan

[3] Department of Virology I, National Institute of Infectious Diseases, Musashimurayama, Tokyo, Japan

[4] Research Institute for Electronic Science, Hokkaido University, Sapporo, Hokkaido, Japan

[#a] Current address: Department of Virology, Graduate School of Medicine and Pharmaceutical Sciences, University of Toyama, Toyama, Toyama, Japan

[#b] Current address: Department of Applied Chemistry, Faculty of Fundamental Engineering, Nippon Institute of Technology, Minamisaitama, Saitama, Japan

* Corresponding author

Noriyo NAGATA, DVM, PhD

Department of Pathology

National Institute of Infectious Diseases

Musashimurayama, Tokyo, Japan

E-mail: nnagata@nih.go.jp;

Tel: +81-42-561-0771 (ext 3361)

Fax: +81-42-561-6572

Abstract

The spike (S) protein of coronavirus, which binds to cellular receptors and mediates membrane fusion for cell entry, is a candidate vaccine target for blocking coronavirus infection. However, some animal studies have suggested that inadequate immunization against severe acute respiratory syndrome coronavirus (SARS-CoV) induces a lung eosinophilic immunopathology upon infection. In this study, we evaluated two kinds of vaccine adjuvants for use with recombinant S protein: gold nanoparticles (AuNPs), which are expected to function as both an antigen carrier and an adjuvant in immunization; and Toll-like receptor (TLR) agonists, which have been previously shown to be an effective adjuvant in a ultraviolet-inactivated SARS-CoV vaccine. All of the mice immunized with more than 0.5 μg S protein without adjuvant escaped from SARS after infection with mouse-adapted SARS-CoV; however, eosinophilic infiltrations were observed in the lungs of almost all of the immunized mice. The AuNP-adjuvanted protein induced a strong IgG response but failed to improve vaccine efficacy or reduce eosinophilic infiltration because of highly allergic inflammatory responses. Whereas similar virus titers were observed in the control animals and the animals

immunized with S protein with or without AuNPs, type 1 interferon and pro-inflammatory responses were moderate in the mice treated with S protein with and without AuNPs. On the other hand, the TLR agonist-adjuvanted vaccine induced highly protective antibodies without eosinophilic infiltrations, as well as Th1/17 cytokine responses. The findings of this study will support the development of vaccines against severe pneumonia-associated coronaviruses.

Key words

coronavirus, adjuvant, immunopathology, eosinophils, mouse model, gold nanoparticles

List of abbreviations

ANOVA analysis of variance

AuNPs gold nanoparticles

BSPP Bis(p-sulfonatophenyl)phenylphosphine dihydrate dipotassium salt

DLS dynamic light scattering

ELISA Enzyme-linked immunosorbent assay

FI-RSV formalin-inactivated respiratory syncytial virus

FBS fetal bovine serum

GM-CSF granulocyte macrophage colony-stimulating factor

HA hemagglutinin

HRP horseradish peroxidase

IFN-γ interferon gamma

IgG immunoglobulin G

IP-10 gamma interferon-induced protein 10

KC neutrophil-related chemokine

MCP-1 monocyte chemotactic protein-1

MEM Minimum Essential Medium Eagle

MERS-CoV Middle East respiratory syndrome coronavirus

MIG monokine induced by gamma interferon

MIP-1α□□ macrophage inflammatory protein 1 alpha

OD optical density

PBS phosphate-buffered saline

PVDF polyvinylidene difluoride

RANTES regulated on activation, normal T cell expressed and secreted

RT room temperature

SARS-CoV Severe acute respiratory syndrome coronavirus

SD standard deviations

SDS-PAGE sodium dodecyl sulfate-polyacrylamide gel electrophoresis

S protein Spike protein

$TCID_{50}$ 50 % tissue culture infectious dose

Th T helper cell

TLR Toll-like receptor

TNF-α tumor necrosis factor alpha

UV ultraviolet

1 INTRODUCTION

Severe acute respiratory syndrome coronavirus (SARS-CoV) (1-6) and Middle East respiratory syndrome coronavirus (MERS-CoV) (7-9) cause severe

pneumonia in humans. Currently, no vaccines or therapeutics are licensed for use against these coronaviruses. The spike (S) protein of coronaviruses binds to cellular receptors and mediates membrane fusion for cell entry (10-12). Antibodies against S protein can block virus binding and fusion, and neutralize virus infection (13-18). Thus, the S protein is a candidate vaccine target for blocking coronavirus infection (11, 18-26). However, some animal studies have suggested that insufficient protective immunity against SARS-CoV may induce an eosinophilic immunopathology in the lungs after the infection (27-29).

Enhanced lung eosinophilic immunopathology became a problem in the 1960s, when a formalin-inactivated respiratory syncytial virus (FI-RSV) vaccine combined with alum adjuvant was injected intramuscularly into children to immunize them against RSV (30-32). This outcome resulted in increased mortality due to enhanced respiratory disease upon subsequent RSV infection in immunized children. This increased mortality is thought to be due to a skewing of the immune response toward a Th2 response with enhanced eosinophil infiltration. In addition, the production of nonprotective antibodies in response to the FI-RSV vaccine may have been due to poor Toll-like receptor (TLR) stimulation (33). In a previous study, we showed that a UV-inactivated SARS-CoV vaccine induced a strong Th2-skewed immune response and that TLR agonists could limit the development of a lung eosinophilic immunopathology (34).

In this study, we produced a recombinant tagged protein containing the ectodomain of the SARS-CoV S protein *via* a baculovirus expression system. We then evaluated the efficacy of the vaccine and its potential to induce a lung eosinophilic immunopathology in our murine SARS model (35). The recombinant S protein-induced antibodies protected against SARS-CoV infection; however, a lung eosinophilic immunopathology was observed in the lungs of immunized mice after SARS infection. Thus, even with the S protein vaccine, an adjuvant is required to prevent lung eosinophilic immunopathology following SARS-CoV infection.

Nanoparticle-based vaccines have been expected to improve vaccine efficacy, immunization strategies, and targeted delivery to promote immune responses (36-38). Gold nanoparticles (AuNPs) have become the choice for immunotherapy applications because their physicochemical properties prevent antibody production against the platform material (36, 39). Furthermore, some *in vitro* and *in vivo* studies have revealed that various immune cells, including macrophages, dendritic cells, and lymphocytes, are stimulated by AuNPs leading to the production of pro-inflammatory cytokines (i.e., IL-1β and TNF-α) and Th1 cytokines (IFN-γ and IL-2) (40). Thus, in this study, we evaluated two kinds of vaccine adjuvants, including AuNPs, which are expected to function as both an antigen carrier and an adjuvant in immunization; and TLR agonists, which have

previously been shown to function as an adjuvant to increase the efficacy of a ultraviolet (UV)-inactivated SARS-CoV vaccine (34).

2 MATERIALS AND METHODS

2.1 Ethics statements

All experiments involving recombinant DNA and pathogens were approved by the Committee for Experiments using Recombinant DNA and Pathogens at the National Institute of Infectious Diseases, Tokyo, Japan. The animal studies were carried out in strict accordance with the Guidelines for Proper Conduct of Animal Experiments of the Science Council of Japan. The animal experiments were conducted in strict compliance with animal husbandry and welfare regulations. All animals were housed in a Japan Health Sciences Foundation-certified facility. All animal experiments were approved by the Committee on Experimental Animals at the National Institute of Infectious Diseases in Japan (approval no. 115101, 116077, and 118124), and all experimental animals were handled in biosafety level 3 animal facilities according to the guidelines of this committee (approval no. 15-32, 16-18, 18-24, and 19-15).

2.2 Cells and viruses

Tn5 cells (BTI-TN-5B1-4 (High Five™)), derived from *Trichoplusia ni* (41-43), were maintained in TC-100 medium (Shima Laboratories, Tokyo, Japan) supplemented with 10% heat-inactivated fetal bovine serum (FBS) (Sigma-Aldrich Japan, Tokyo, Japan) and 1% kanamycin (Thermo Fisher Scientific, Waltham, MA) and 2% tryptose phosphate broth (Thermo Fisher Scientific) at 27℃. Insect Sf9 cells, derived from *Spodoptera frugiperda* (41-43), were kindly provided by Dr. Yoshiharu Matsuura (Osaka University, Osaka, Japan), and were maintained in Sf-900II SFM (Thermo Fisher Scientific) supplemented with 10% heat-inactivated FBS and 1% kanamycin (Thermo Fisher Scientific) with incubation at 27℃.

Vero E6 cells, derived from the African green monkey kidney (ATCC No. CRL-1586, American Type Cell Collection, Manassas, VA) were cultured in Minimum Essential Medium Eagle (Sigma-Aldrich Japan) containing 5% FBS (Sigma-Aldrich Japan), 50 IU/ml penicillin G, and 50 μg/ml streptomycin (Thermo Fisher Scientific) (5% FBS-MEM). Stocks of a mouse-passaged Frankfurt 1 isolate of SARS-CoV, F-musX-VeroE6, were propagated twice and titrated on Vero E6 cells prior to cryopreservation at -80℃, as previously described (35). Viral infectivity titers are expressed as the 50 % tissue culture infectious dose ($TCID_{50}$)/ml on Vero E6 cells and were calculated according to the Behrens–

Kärber method. All work with infectious SARS-CoV was performed under biosafety level 3 conditions.

2.3 Recombinant SARS S protein

Recombinant coronavirus S protein was prepared using a baculovirus expression system as described previously (41, 44). The sequence of the coronavirus S protein was obtained from the SARS-CoV Frankfurt 1 strain (NCBI accession no. AY291315). The nucleotide sequence encoding amino acids 1-1194 of the SARS-CoV S protein ectodomain was tagged at the C-terminus with a Strep-tag and an 8xHis-tag, and cloned into the transfer vector pAcYM1 (kindly provided by Dr. Y. Matsuura, Osaka University (42)). The predicted molecular weight of the recombinant S protein was 135 kDa. Recombinant baculovirus was produced in insect Sf9 cells using BD Baculo Gold Linearized Baculovirus DNA (BD Biosciences, Franklin Lakes, NJ) with UniFector reagent (B-Bridge International, Santa Clara, CA) according to the manufacturer's instructions. Next, insect Tn5 cells were infected with the recombinant baculovirus to produce recombinant S protein. Four days after the infection, the recombinant S protein was purified from the culture supernatant via affinity chromatography using an ÄKTAprime plus system with PrimeView software (GE Healthcare Japan, Tokyo, Japan) and then collected using a HisTrap excel column (GE Healthcare Japan).

2.4 Protein analysis

The purified protein was heated in sample buffer solution with 2-Mercaptoethanol (Wako, Tokyo, Japan) at 90℃ for 3 min and then size fractionated via Sodium dodecyl sulfate-polyacrylamide gel electrophoresis (SDS-PAGE) on a 4 - 12% polyacrylamide gel (Thermo Fisher Scientific). The proteins were then stained with Coomassie Brilliant Blue staining solution (Bio-Rad, Hercules, CA).

For western blotting, proteins fractionated via 4 - 12% SDS-PAGE were transferred to a polyvinylidene difluoride (PVDF) membrane (Merck Millipore, Burlington, MA). The membrane was incubated in blocking reagent (TOYOBO, Osaka, Japan) for 1 h at room temperature (RT) to improve the signal. A rabbit antibody against SARS S glycoprotein (ab22156, abcam, Cambridge, UK) (1:500) and the anti-His-tag mouse horseradish peroxidase (HRP)-DirecT antibody (OGHis; D291-7, MBL Life Science, Nagoya, Japan) (1:5000) were used as the primary antibodies. After incubation with the primary antibodies for 1 h at RT, the membrane was treated with a HRP-conjugated secondary antibody (ab7090, abcam) (1:4000) for 1 h at RT. After washing with 0.05% Tween 20 in Tris-buffered saline (Wako), the proteins were detected using Immobilon Western Chemiluminescent HRP Substrate (Merck Millipore), and images were captured with an LAS 4000 Luminescent Image Analyzer (Fujifilm, Tokyo, Japan). The

concentration of the purified protein was measured using a Pierce BCA Protein Assay Kit (Thermo Fisher Scientific) and the Nano Drop 1000 microvolume UV-Vis spectrophotometer (Thermo Fisher Scientific).

2.5 AuNP-protein complex (S+AuNP)

2.5.1 Conjugation of protein to AuNPs

Bis(p-sulfonatophenyl)phenylphosphine dihydrate dipotassium salt (BSPP) coating of gold nanoparticles was carried out according to the previous literature with some modifications (45). AuNPs were prepared as a commercial gold colloid with diameters of 40 nm (EMGC40, BBI Solutions, South Wales, UK) and 100 nm (EMGC100, BBI Solutions). BSPP (5 mM for 40 nm AuNPs, 7.5 mM for 100 nm AuNPs) (Merck Millipore) was mixed with the gold colloid (particle concentration, 0.15 nM) overnight at RT with shaking. After centrifugation of the mixture two times at 2000 × *g* for 10 min to remove the excess BSPP, the pellet was re-suspended in distilled water at a concentration of 0.25 nM. The AuNPs were passed through a 0.22 μm filter (MILLEX-GV, Merck Millipore). The purified recombinant S protein was added to the BSPP-coated AuNPs, and the mixture was incubated at RT for 1 h for adsorption. Dynamic light scattering (DLS) was measured using a hydrodynamic diameter (ELSZ-2000, Otsuka Electronics, Osaka, Japan). Measurements were performed at 25℃in a disposable UV cuvet

(UVC-Z8.5, VIOLAMO, AS ONE, Osaka, Japan) using a sample volume of 100 μL. For animal immunization, the mixture was added to 3-fold-diluted phosphate-buffered saline in distilled water (3× PBS). To maintain the final concentrations of the protein with AuNPs for animal immunization, we used the mixture without further purification (i.e., the mixture after centrifugation and wash with PBS).

2.5.2 Quantification of the AuNP-adsorbed protein

After adsorption of 0.1 μg S protein with 2 fmol of 40-nm AuNPs in 3× PBS (referred to as S+AuNPs), the protein on the AuNPs was quantified. The S+AuNP solution was concentrated via centrifugation at 2000 × *g* for 10 min at RT, and the supernatant was then removed (Sup1). After washing with 3× PBS twice (Sup2), the pellet was re-suspended in 3× PBS, and SDS-PAGE sample buffer was added to extract the proteins from the surface of the AuNPs. After heating at 95℃ for 5 min to denature the proteins, the solution was centrifuged at 6000 × *g* for 5 min at RT to completely precipitate the AuNPs (Binding S). The supernatants were subjected to SDS-PAGE with S protein samples of known concentrations (S protein was adjusted to 5 ng/μl, and 50 ng/lane was subjected to SDS-PAGE followed by western blotting) and then analyzed via western blotting with an anti-His antibody.

The immunoreactive proteins were detected and quantified via densitometry using a 4000 Luminescent Image Analyzer (Fujifilm).

2.5.3 Electron microscopy

Purified S protein, AuNPs, and S+AuNPs in 3× PBS were observed under transmission electron microscopy. Samples on glow-discharged carbon-coated Cu grids (Veco grids; Nisshin EM, Tokyo, Japan) were stained with 2% phosphotungstic acid (Wako). Data were collected using an HT7700 transmission electron microscope (Hitachi, Tokyo, Japan) operating with an electron beam at 80 kV and a magnification of 10,000.

2.6 Animal experiments

2.6.1 Immunization

To confirm the immunogenicity of the purified recombinant S protein, BALB/c mice (female, 6-week-old (Japan SLC, Shizuoka, Japan); n = 6–7; total, 25) were immunized subcutaneously twice at 2 week intervals with 1 μg, 0.5 μg, 0.1 μg, or 0.05 μg doses of the protein in 100 μL PBS.

To evaluate the final concentrations of AuNPs and S protein for animal immunization, S protein was added to a 0.1 nM solution of BSPP-coated AuNPs. The final concentrations of the protein with AuNPs for animal immunization were

as follows: for experiment #1, 0.5 μg of S protein in a 0.1 nM solution of AuNPs was prepared and diluted 5-fold or 10-fold. Immunization doses per mouse were as follows: 0.5 μg S protein with 10 fmol AuNPs, 0.1 μg S protein with 2 fmol AuNPs, and 0.05 μg S protein with 1 fmol AuNPs; for experiment #2, 0.5 μg, 0.1 μg, or 0.05 μg of S protein with 10 fmol AuNPs. The animal experiments were conducted by subcutaneously immunizing BALB/c mice (7-week-old, female; n = 6–7, total 38 mice) at approximately 3 week intervals.

To evaluate the optimum AuNP diameter for animal immunization, 100 nm and 40 nm AuNPs were prepared. Purified S protein with 2 fmol BSPP-coated AuNPs was used for immunization. BALB/c mice (7-week-old, female; n = 6–7, total 13) were subcutaneously immunized twice at 2 week intervals.

To assess the effects of the adjuvants, the purified S protein was formulated with AuNPs or TLR agonists at 0.1 μg per dose. The TLR agonists consisted of 1 μg lipopolysaccharide (LPS) (Sigma-Aldrich, St. Louis, MO), 2.5 μg poly(I:C) (Invitrogen, San Diego, CA), and 0.1 μg poly(U) (Invitrogen) in PBS per immunization (33, 34). Female BALB/c mice (female, 13-week-old; Japan SLC, n = 6–7, total, 26) were subcutaneously immunized twice at 2 week intervals with S+AuNPs, S+TLR, S protein, or PBS.

Control mice were subcutaneously injected with PBS with or without 2 fmol AuNPs twice at 2 week intervals. Two weeks after each immunization, serum samples were collected from all mice for measurement of the antibody response.

2.6.2 Virus infection of immunized mice

Approximately 3 weeks after the second immunization, mice were anesthetized via intraperitoneal injection of a mixture of 1.0 mg ketamine (Daiichi Sankyo Company, Tokyo, Japan) and 0.02 mg xylazine (Byer Japan, Osaka, Japan) (0.08 ml/10 g of body weight). These mice were then inoculated intranasally with SARS-CoV (10^6 $TCID_{50}$ in 30 μl of 2% FBS-MEM). The infected mice were then observed for clinical signs of infection, and their body weight was measured daily for 10 days (n = 6–7 mice; total, 51 immunized mice). To analyze viral replication, cytokine expression, and pathology, animals were sacrificed at various time points after inoculation (n = 3–5 mice per group; total, 51).

Viral inoculations were performed under anesthesia, and all efforts were made to minimize potential pain and distress. After inoculation, animals were monitored once a day during the study. The humane endpoint was defined as the appearance of clinically diagnostic signs of respiratory stress, including respiratory distress and weight loss of more than 25%. Animals were euthanized under

anesthesia with an overdose of isoflurane if severe disease symptoms or weight loss was observed.

2.7 Virus titration

Lung tissue homogenates (10%, wt/vol) were prepared in 2% FBS-MEM. Samples were clarified via centrifugation at 740 *g* for 20 min, and the supernatant was inoculated onto Vero E6 cell cultures for virus titration.

2.8 Antibody assays

Sera were obtained from pre-immunized mice and immunized mice 2 weeks after the second immunization. After inactivation of the serum samples at 56℃for 30 min, they were stored at -80℃until the assays were performed.

2.8.1 Enzyme-linked immunosorbent assays (ELISAs)

To assess the specificity of the IgG produced by the immunized mice, recombinant SARS-CoV S protein (for antigen-specific IgG) and UV-inactivated SARS-CoV (for virus-specific IgG) were used as ELISA antigens. These antigens were used in conventional ELISAs as described previously (34). Briefly, 96-well assay plates (Corning Inc., Corning, NY) were coated with 50 ng of purified S protein or 4 μg of UV-inactivated SARS-CoV in a coating buffer (pH 7.4; Thermo Fischer Scientific). The plates were then washed three times with PBS containing 0.05%

Tween 20 (Sigma-Aldrich) (PBS-T). BlockAce (DS Pharma Biomedical K.K., Osaka, Japan) was added to each well, and the plates were incubated for 2 h at 37℃. The serum samples were serially diluted (10-fold or 2-fold) in PBS-T with 4× BlockAce from 1:10 to $1:10^{10}$ for the antigen-specific IgG ELISA or from 1:10 to 1:5120 for the virus-specific IgG ELISA. The diluted samples were added to the plates, which were then incubated for 1 h at 37℃. After three washes with PBS-T, the wells were further incubated with HRP-conjugated anti-mouse IgG (Thermo Fischer Scientific) antibody (diluted 1:1000 in PBS-T with 4× BlockAce). After three washes with PBS-T, ABTS substrate (Roche, Basel, Switzerland) was added to the wells, and the plates were incubated for 30 min at 37℃. The optical density (OD) of each well was measured at 405 nm using a microplate reader (Model 680, Bio-Rad). The cut-off value calculated from the mean OD value plus three standard deviations (mean + 3SD) was determined for each dilution using serum samples from pre-immunized mice. The IgG titer was defined as the reciprocal of the highest dilution at which OD value was higher than the cut-off value.

2.8.2 Neutralizing antibody test

Serum samples were 2-fold diluted over a range of 1:4 to 1:256 in 2% FBS-MEM. Each sample was mixed with virus solution (F-musX-VeroE6 of 100 $TCID_{50}$ per well), and the mixtures were incubated for 1 h at 37℃ for neutralization. After

incubation, the mixtures were inoculated onto monolayers of VeroE6 cells in 96-well culture plates, followed by incubation at 37℃with 5% CO_2 for 3 days. The cells were then examined for cytopathic effects. The sera titers of neutralizing antibodies were calculated as the reciprocal of the highest dilution at which no cytopathic effects were observed.

2.9 Histopathology and histochemistry

Mice were anesthetized and perfused with 2 ml of 10% phosphate-buffered formalin (Wako). The lungs were harvested, fixed, embedded in paraffin, sectioned, and stained with hematoxylin and eosin. Eosinophils were identified via Astra Blue/Vital New Red staining, a combined eosinophil/mast cell stain (C.E.M. Stain Kit; DBS, Pleasanton, CA). Using the Astra Blue/Vital New Red-stained slides, the peribronchiolar area in five 147,000-μm^2 sections was assessed by light microscopy using a DP71 digital camera and cellSens software (Olympus, Tokyo, Japan), and the numbers of eosinophils counted in the lungs of each mouse were averaged as previously described (34).

2.10 Detection of inflammatory cytokines and chemokines

The levels of cytokines and chemokines in mouse lung homogenates (10%, wt/vol) were measured using a custom mouse cytokine/chemokine magnetic bead panel

96-well plate assay kit (Milliplex MAP kit, Merck Millipore), which includes 21 cytokines and chemokines: eotaxin, interferon gamma (IFN-γ), IL-1α, IL-1β, IL-2, IL-4, IL-5, IL-6, IL-10, IL-12p40, IL-12p70, IL-13, IL-17, gamma interferon-induced protein 10 (IP-10), neutrophil-related chemokine KC (KC), monocyte chemotactic protein-1 (MCP-1), macrophage inflammatory protein 1 alpha (MIP-1α), granulocyte macrophage colony-stimulating factor (GM-CSF), monokine induced by gamma interferon (MIG), regulated on activation, normal T cell expressed and secreted (RANTES), and tumor necrosis factor alpha (TNF-α). The assay samples were read on a Luminex 200™ instrument with xPONENT software (Merck Millipore), as described by the manufacturer.

2.11 Quantitative real-time RT-PCR

To measure the levels of type 1 IFN mRNA expression, RNA was extracted from 10% (w/v) lung homogenates from virus-infected mice using an RNeasy Mini Kit (Qiagen, Hilden, Germany) according to the manufacturer's instructions. The levels of mRNAs encoding IFN-α and IFN-β were examined via real-time RT-PCR using an ABI Prism 7900HT Fast real-time PCR system (Applied Biosystems, Foster City, CA). The TaqMan probes and primers were as follows; IFN-α4 (forward, CAACTCTACTAGACTCATTCTGCAAT; reverse, AGAGGAGGTTCCTGCATCACA; probe,

ACCTCCATCAGCAGCTCAATGACCTCAAA), IFN-β (forward, GCTCCTGGAGCAGCTGAATG; reverse, TCCGTCATCTCCATAGGGATCT; probe, TCAACCTCACCTACAGGGCGGACTTC), and β-actin (forward, ACGGCCAGGTCATCACTATTG; reverse, CAAGAAGGAAGGCTGGAAAAGA; probe, CAACGAGCGGTTCCGATGCCC). The reaction conditions have been described previously (34, 46). Briefly, reaction mixtures were incubated at 50℃ for 30 min, followed by an incubation 95℃ for 15 min and thermal cycling, consisting of 40 cycles of denaturation at 94℃ for 15 s, and annealing and extension at 60℃ for 60 s. The expression of each gene was normalized to that of β-actin.

2.12 Statistical analysis

Data are expressed as the mean and standard error of the mean. The statistical analyses were performed using Graph Pad Prism 8 software (GraphPad Software, La Jolla, CA). Body weight curves, virus titers, eosinophil counts, and multiplex assay results were analyzed using one-way or two-way analysis of variance (ANOVA). Tukey's multiple comparisons test was used to compare the results from each group. The results of the antibody titer assays were analyzed using non-parametric tests, i.e., Dunn's multiple comparisons test following the Kruskal-Wallis test. A p-value <0.05 was considered statistically significant.

3 RESULTS

3.1 Expression of recombinant tagged S protein

We generated a recombinant tagged protein that included the ectodomain of the SARS-CoV S protein using a baculovirus expression system. S protein of SARS-CoV contains a large amino-terminal ectodomain and a short carboxy-terminal endodomain bridged with a hydrophobic transmembrane domain (Figure 1a). The ectodomain of the S protein is extensively glycosylated with N-linked glycosylation and has been reported to be important for interactions with receptors on the surface of host cells (14, 47). In addition, to avoid insoluble protein expression caused by numerous hydrophobic amino acids, the transmembrane domain including the carboxy-terminal endodomain was removed from the recombinant spike protein (Figure 1a). Higher expression was obtained from a construct encoding a recombinant SARS-CoV S protein containing a Strep-8x his-tag at the carboxyl terminus compared with that obtained from an 8x his-tagged construct. After purification of the recombinant tagged protein from culture supernatant *via* gel filtration chromatography, the identity of the recombinant protein, with an expected molecular weight of 135 kDa, was confirmed via SDS-PAGE and western blotting (Figure 1b).

3.2 Immunogenicity of the recombinant tagged SARS-CoV S protein in mouse

To confirm the immunogenicity of the recombinant SARS-CoV S protein, purified protein was used for immunization into BALB/c mice. Groups of 6-7 mice were immunized with different amounts of recombinant S protein (1.0, 0.5, 0.1, or 0.05 μg per immunization) and then challenged with mouse-adapted SARS-CoV. Two weeks after the second immunization with the SARS-CoV S protein, the dose-dependency of the antigen-specific IgG production was assessed in all of the immunized mice (Figure 2a). Approximately 6 weeks after the second immunization, all of the mice (12-weeks-old at the time of the challenge) were intranasally inoculated with mouse-adapted SARS-CoV. Non-immunized animals showed body weight reductions of approximately 17% compared with the initial body weight, and four out of six mice were moribund and were euthanized within 5 days post-inoculation (d.p.i.) (Figure 2b). Two animals were fully recovered by 6 d.p.i. On the other hand, all of the immunized animals showed body weight loss within 2 d.p.i., and the animals in the 1.0 μg- and 0.5 μg-immunized groups recovered by 4 d.p.i.; however, three out of seven mice in the 0.1 μg-immunized group and three out of six in the 0.05 μg-immunized group did not recover and were moribund. Animals that survived fully recovered by 5 or 6 d.p.i. In summary, all of the 1.0 μg- and 0.5 μg-immunized mice survived the infection with a lethal

dose of mouse-adapted SARS-CoV, while the mice in the 0.1 μg- and 0.05 μg-immunization groups did not (Figure 2c). Three out of seven mice in the 0.1 μg-immunized group and three out of six in the 0.05 μg-immunized group were moribund and were euthanized within 6 d.p.i. No animals were sacrificed before meeting the criteria for euthanasia.

In addition, we found eosinophilic infiltrations around the bronchioles in the lungs from almost all of the immunized mice 10 days after the challenge infection with SARS-CoV (Figure 3a, b). From our previous work with a UV-inactivated SARS-CoV immunization model, we speculated that insufficient immunization with the recombinant S protein induced the eosinophil infiltration in the lungs upon infection with mouse-adapted SARS-CoV in this BALB/c mouse model (34). Therefore, we next investigated the efficacy of vaccine adjuvants.

3.3 Efficacy of adjuvants on vaccine immunogenicity

We examined the effects of two types of vaccine adjuvants: AuNPs, which are used as antigen carriers and adjuvants for subunit vaccines (the S+AuNP-immunized group); and TLR agonists (the S+TLR-immunized group). The recombinant S protein was used at 0.1 μg/mouse for immunization.

Conjugation of S protein to AuNPs was confirmed by detecting changes in the diameter of the AuNPs after BSPP coating and S protein binding by DLS (Table 1). Then, the optimal AuNP concentration was determined by measuring the virus-specific Ig G response (UV-inactivated SARS-CoV was used as the ELISA antigen) after the second immunization. Stable results were obtained when 0.1 μg S protein + 2 fmol AuNPs were used to immunize BALB/c mice (Figure 4a, b). We also evaluated the influence of the diameter of the AuNPs on animal immunization. The effects of the size and shape of the AuNPs on the immunological response was previously evaluated in a study of West Nile virus envelope protein (WNV-E protein) (39). WNV-E protein-coated 40 nm spherical AuNPs induced sufficient levels of WNV-E-specific antibodies. The WNV particle is around 40 nm in diameter. We evaluated 100 nm spherical AuNPs with a modified SARS-CoV particle, ranging from 50 to 200 nm in diameter (48). Animal experiments revealed that there were no differences in the IgG response when spherical AuNPs with diameters between 40 and 100 nm were used for the immunization (Figure 4c). We used 0.1 μg S protein with 2 fmol of 40-nm AuNPs in the following experiments.

The amount of protein on the AuNPs was quantified via western blot analysis after adsorption of S protein to AuNPs (Figure 4d). We calculated the ratio of the amount of AuNP-bound protein to the amount of free protein in the S+AuNP solution via chemiluminescence-based western blotting. Images were captured

using an LAS 4000 Luminoimage analyzer (Fujifilm) and then analyzed using the ImageQuant TL software (GE Healthcare). The percentage of protein bound to the AuNPs was 28.3 + 5.9% (5 experiments). In addition, the structure of the S+AuNPs was examined by transmission electron microscopy (Figure 4e), which confirmed S protein binding to the AuNPs and the presence of free S protein in solution.

We next evaluated the efficacies of the adjuvants. We used 13-week-old mice for immunization, and these animals were 18 weeks old at the time of the challenge infection. Two weeks after the second immunization, the levels of antigen-specific IgG were measured in all of the immunized groups, and the levels were significantly higher in both the S+AuNP- and S+TLR-immunized groups compared with that in the S protein-immunized group (Figure 5a). We also confirmed virus-specific seroconversion in these mice. When UV-inactivated SARS-CoV was used as an ELISA antigen, all of the S+TLR-immunized mice showed significantly higher titers of virus-specific IgG, which were low in the S+AuNP-immunized mice (Figure 5b). Similar results were obtained from the neutralizing antibody analysis (Figure 5c).

Three weeks after the second immunization, all of the animals were intranasally inoculated with SARS-CoV (n = 6 or 7). Within 2 d.p.i., all of the mice

showed ruffled fur and body weight loss, and all of the non-immunized animals showed body weight reductions of more than 20% and were moribund within 5 d.p.i. (n = 6) (Figure 5d, e). Two mice died of pulmonary edema before meeting the criteria for euthanasia. All of the S+TLR-immunized mice recovered within 4 d.p.i.; however, four out of seven of the S+AuNP-immunized mice and two out of six of the S protein-immunized mice were moribund within 6 d.p.i. (Figure 5d, e). Four mice in the S+AuNP- and S protein-immunized groups died of pulmonary edema before meeting the criteria for euthanasia.

From these results, it was clear that S+AuNP immunization induced high levels of antigen-specific IgG but weak production of virus-specific IgG and neutralizing antibodies against SARS-CoV. Thus, the protective ability of the S+AuNP vaccine was lower than that of the S+TLR vaccine.

3.4 Effects of the adjuvants on lung eosinophilic immunopathology

Histopathological investigation revealed that eosinophilic infiltrations occurred in the lungs of both S protein- and S+AuNP-immunized mice but not in the lungs of the animals in the S+TLR-immunized group 10 d.p.i. (Figure 6). We also investigated the histopathology of mice pretreated with AuNPs, but no eosinophil infiltration was observed after SARS-CoV infection (AuNPs in Figure 6a, b).

We next used mouse lung homogenates to investigate the viral kinetics and immune reaction on days 1, 3, and 5 p.i. The virus titers were initially low and then decreased in the lungs of the S+TLR-immunized mice, and the others showed approximately equal titers (Figure 7a). High levels of type 1 interferon, IFN-α4 and IFN-β, were detected in the lungs of non-immunized mice, but lower or delayed responses were observed in the animals in the S protein- and S+AuNP-immunized groups. No response was detected in the animals in the S+TLR-immunized group (Figure 7b).

We also investigated the cytokine and chemokine responses in the lungs (Figure 8). The levels of pro-inflammatory cytokines, including IL-12p40, IL-1α, IL-1β, TNF-α, and GM-CSF, were elevated 1 d.p.i. in the control mice. The vaccinated mice showed moderate induction of these pro-inflammatory cytokines and chemokines. The levels of IL-6 and KC were only elevated in the control mice 3 d.p.i. The levels of several macrophage-related chemokines (MCP-1, MIP-1α, and IP-10) were higher in the control, S protein- and S+AuNP-immunized mice at 3 d.p.i. than in the S+TLR-immunized mice. RANTES was induced at 1 d.p.i. in the control, S protein- and S+AuNP-immunized mice but was delayed in the S+TLR-immunized mice. Th1 cytokine production and IL-10 responses following IL-2 and IFN-γ induction were observed in the S protein- and S+AuNP-immunized mice on day 3 p.i. High production of allergic inflammation-related cytokines and

other chemokines, including IL-4, IL-5, and eotaxin, was observed in the S protein- and S+AuNP-immunized mice within 5 d.p.i. In addition, the levels of IL-13 were higher in the S protein- and S+AuNP-immunized mice than in the control and S+TLR-immunized mice. Significant differences in the levels of IL-1α, MIP-1β, IL-2, IFN-γ, and IL-4 were detected in the S protein- and S+AuNP-immunized mice. S+TLR-immunized mice showed higher levels of GM-CSF on day 3 p.i. and IL-17 within 5 d.p.i. compared with the respective levels in the other immunized groups. Other cytokine and chemokine responses were moderate or absent in the S+TLR-immunized mice.

Overall, each group of mice showed different types of immune responses in the lungs during the early phase of SARS-CoV infection. Non-immunized mice showed a pro-inflammatory response during the early phase of infection. The S- and S+AuNP-immunized mice showed Th1 and Th2 responses accompanied by allergic inflammation. Th1- and Th17-biased cytokine induction was observed in the S+TLR-immunized mice.

4 DISCUSSION

In the development of vaccine candidates against coronavirus infection, subunit vaccines, viral vector vaccines, and DNA vaccines targeting the viral S protein have been shown to be very effective *in vivo* (11, 19, 21, 23, 25, 26, 49-55).

Subunit vaccines are considered highly safe products because they use antigenic components without the need to introduce viral particles (56). Furthermore, it is possible to induce cellular and humoral immune responses and high-titer neutralizing antibodies when antigens are combined with appropriate adjuvants (26, 56). Researchers have previously produced recombinant baculovirus-expressed SARS-CoV S protein and showed that it could be used to induce high production of neutralizing antibodies in mice (22, 26). However, lung eosinophilic immunopathology was not evaluated in these studies.

Honda-Okubo et al. reported that immunization with a commercial recombinant S protein, NR-722 (Protein Science Corp., Meriden, CT), which is produced in insect cells, with or without alum adjuvant, resulted in lung eosinophilic immunopathology after SARS-CoV infection (intramuscularly, twice with 1.0 μg S protein) (28). They succeeded in avoiding the immunopathology induced by the vaccine by combining it with a delta insulin-based polysaccharide adjuvant. The adjuvant induced IFN-γ responses, suggesting that an inadequate vaccine-induced Th1 response caused the lung eosinophilic immunopathology (28). This was also observed previously by Agrawal et al, who reported that inactivated MERS-CoV vaccination leads to a lung eosinophilic immunopathology and IL-5 and IL-13 production upon live virus challenge in transgenic mice bearing

the human CD26/DPP4 receptor (57). Severe pneumonia related coronaviruses such as SARS-CoV and MERS-CoV could induce the same pathology.

In this study, we explored the potential of AuNPs to be used as an adjuvant to promote immune responses with balanced effects on Th1 and Th2 T-cell immunity (36, 39, 40). AuNPs stimulate macrophages, dendritic cells, and lymphocytes after induction of pro-inflammatory cytokine (i.e., IL-1β and TNF-α) and Th1 cytokine (i.e., IFN-γ and IL-2) expression (40). Niikura et al. demonstrated that AuNP-adjuvanted West Nile virus E protein (10 μg) showed high antigenicity in mice and induced inflammatory cytokine production, including TNF-α, IL-6, IL-12, and GM-CSF, by antigen-presenting cells *in vitro* (39). Indeed, AuNP-adjuvanted S protein induced strong IgG responses to S protein itself in this study; however, it failed to induce protective immune responses and limit eosinophilic infiltrations after virus challenge. One explanation for the failure to induce protective immune responses could be that structural changes in S protein upon binding to the AuNP adjuvant resulted in S-binding IgGs that were unable to neutralize the virus (58). AuNPs and S protein bind together via electrostatic interactions and S-protein forms a "protein corona" around AuNPs (59, 60). Indeed, both DLS and TEM structure analysis indicated that the conjugated S protein on AuNPs formed a protein corona, which is considered to result in structural changes in adsorbed proteins (59) for adaptation to the nanoparticle surface and surrounding

environment (61). Protein secondary structure is strongly affected by the surface charge of AuNPs (62). The particle surface of a protein corona defines the biological identity of the particle when it is attached to the cell surface *in vivo* (58, 59). Thus, even a small modification in S protein structure could impact both negatively and positively its immunogenicity. More work will be required to study the mechanisms and test whether the AuNP-adjuvanted vaccine is effective against coronavirus infection (i.e., effect of antigen binding methods, antigen against the receptor binding site).

Cytokine and chemokine analysis revealed that each group of mice had different lung immune responses early after SARS-CoV infection. While similar virus titers were observed in the lungs of non-, S protein- and S+AuNP-immunized mice, type 1 IFN and pro-inflammatory responses were moderate in both the S protein- and S+AuNP-immunized mice. After infection, type 1 IFNs are secreted by infected cells, macrophages, and dendritic cells to counteract viral infection (63, 64). Type 1 IFNs upregulate pro-inflammatory cytokines and chemokines, including IL-12 (63). The macrophage-related chemokine responses were similar among the non-, S protein-, and S+AuNP-immunized mice; however, the Th1 and Th2 responses were higher in the S protein- and S+AuNP-immunized mice. The cells may also moderate pro-inflammatory reactions in the animals in these groups. Interestingly, although S protein-immunized mice showed significant protection

against SARS-CoV infection, the virus titers remained higher than those in non-immunized mice. In adult mouse models of SARS-CoV infection, the excessive host innate immune responses contributing to SARS-CoV lung pathology are complex and involve changes in activated macrophages and neutrophils (65-67). We previously reported that IFN-γ treatment 3 hours after inoculation protected mice from severe SARS-CoV-induced pulmonary edema that otherwise results in the death of uninoculated adult mice (35). However, the virus titer in the lungs did not differ between IFN-γ-treated and PBS-treated adult mice. In this study, S protein-immunized mice showed an IFN-γ response on day 1 p.i. Thus, we speculated that IFN-γ induction may contribute to protection against SARS in the S protein immunized mice.

PBS pre-treated challenge control mice showed very slight changes in the bronchi area of lungs after SARS-CoV infection (Figure 3a and 6b). The pathological changes in SARS-CoV-infected lungs, including diffuse alveolar damage, are mainly seen in the alveolar area (35). However, eosinophil infiltrations occur around middle size blood vessels in the bronchi area. Thus, we demonstrated the bronchi area from animals in these figures whereas small changes (i.e. a few inflammatory cell infiltrations around the blood vessels with edema) were observed in the bronchi area of the control mouse. The histopathological findings of eosinophil infiltration around the bronchiole on day 10 p.i. were correlated with

high production of allergic inflammation cytokines, i.e., IL-13, IL-4, IL-5, and eotaxin, in both the S protein- and S+AuNP-immunized mice. These findings suggest that the amount of antibody generated against SARS-CoV was not sufficient to orchestrate immune responses, including innate immunity and Th2-skewed responses, during the infection.

In this study, AuNPs did not show dose dependency in eliciting immune responses. When low-molecular weight poly(I:C)s were conjugated with gold nanorods as adjuvants for intranasal hemagglutinin (HA) influenza vaccination, low doses of AuNPs (i.e., 1 fmol) were more effective in reducing virus replication in a nasal wash than 10-fold higher doses of gold nanorods (i.e., 10 fmol) (68). On the other hand, Mottram et al. showed that the nanoparticle size of carboxyl-modified polystyrene beads carrying whole ovalbumin influenced Th1 and Th2 immune reactions. When 40-50 nm beads were used to vaccinate mice, high IFN-γ induction was observed, whereas 93-123 nm beads induced IL-4 production (69). Although we did not evaluate in detail the influence of the amount and size of AuNPs, the amount and size of AuNPs should be carefully considered if nanoparticle vaccine platforms are used for the development of coronavirus vaccines.

In this study, we expressed S protein via a recombinant baculovirus system. Purification of recombinant SARS-CoV S protein was more effective when expression was from a construct containing a Strep-8x his-tag at the S protein carboxyl terminus than when a 8x his-tagged construct was used. The purification was conducted only via His trap purification using affinity chromatography to minimize protein loss. After the second immunization with the purified recombinant S protein, high IgG levels against immunogen-specific IgG were detected in the murine sera, and they were protective against SARS-CoV infection *in vivo* (subcutaneously, twice with 1.0 or 0.5 μg of S protein). The purified protein showed high immunogenicity in BALB/c mice but did not prevent eosinophilic infiltrations.

Mice of different ages were used in this study. Young adult mice (6 or 7-week-old, female) were used to confirm the immunogenicity of recombinant S protein and S+AuNP and adult mice (13-weeks-old; challenged at 17-weeks-old) were used for the challenge experiment. There were significant differences in the levels of the virus-specific IgG titer in mice immunized with 0.1 μg of S+AuNP between Figure 4a and 5b. We speculate that the difference could be due to differences in the ages of the mice employed in these experiments. In general, young adult (around 6-weeks-old) mice show more robust immune responses than old mice, and the robustness of the immune response decreases with age (70). In

addition, the intervals between first immunization and the time-points of sera collection were different. We conducted a minimum dose immunization of adult BALB/c mice with the S protein (subcutaneously, twice with 0.1 μg S protein). 0.1 μg of TLR agonist-adjuvanted S protein induced a sufficiently high expression of neutralizing antibodies and prevented the eosinophilic infiltrations. After SARS-CoV infection, induction of GM-CSF, RANTES, IL-10, IL-2, MIG, and IL-17, but not Type 1 IFN expression was detected in the lungs of S+TLR-immunized mice that had sufficient antiviral antibodies. Interestingly, only the S+TLR-immunized mice showed high levels of IL-17 within 5 d.p.i., suggesting that a Th17 response occurred in the lungs during SARS-CoV infection in the presence of neutralizing antibodies. Interestingly, a Th1/Th17 bias in cytokine induction was also observed in a study of SARS-CoV S protein when delta insulin was used as an adjuvant (28). The activation of specific T-cell subsets by adjuvants may be critical to ensure vaccine efficacy and eosinophilic immunopathology upon SARS-CoV infection.

Overall, AuNP-adjuvanted S protein induced an antigen-specific IgG response but failed to induce a protective antibody and limit eosinophilic infiltration in the lungs. On the other hand, the TLR agonists successfully minimized the amount of recombinant S protein required for the vaccination to 0.1 μg, and increased vaccine immunogenicity and reduced eosinophilic infiltration in

the lungs after the SARS-CoV challenge infection in our mouse model. To prevent insufficient immunization against SARS-CoV, even with an S protein-based vaccine, appropriate adjuvant development is needed. The findings of this study will support the development of vaccines not only against SARS-CoV infection but also against other severe pneumonia-related coronaviruses, likely including MERS-CoV.

ACKNOWLEDGMENTS

We appreciate technical assistance from Ms. Chie Takeuchi at Hokkaido University. We thank Drs. Hideki Asanuma, Shin-ichi Tamura, and Akira Ainai (National Institute of Infectious Diseases) for helpful discussions. We also thank our colleagues at the Institute, especially Ms. Midori Ozaki, for their technical assistance.

DISCLOSURE

The authors declare that they have no conflicts of interest regarding this manuscript.

REFERENCES

1 Drosten, C., Gunther, S., Preiser, W., Van Der Werf, S., Brodt, H.R., Becker, S., Rabenau, H., Panning, M., Kolesnikova, L., Fouchier, R.A., Berger, A.,

Burguiere, A.M., Cinatl, J., Eickmann, M., Escriou, N., Grywna, K., Kramme, S., Manuguerra, J.C., Muller, S., Rickerts, V., Sturmer, M., Vieth, S., Klenk, H.D., Osterhaus, A.D., Schmitz, H., Doerr, H.W. (2003) Identification of a novel coronavirus in patients with severe acute respiratory syndrome. *N Engl J Med* **348:** 1967-76.

2 Guan, Y., Peiris, J.S., Zheng, B., Poon, L.L., Chan, K.H., Zeng, F.Y., Chan, C.W., Chan, M.N., Chen, J.D., Chow, K.Y., Hon, C.C., Hui, K.H., Li, J., Li, V.Y., Wang, Y., Leung, S.W., Yuen, K.Y., Leung, F.C. (2004) Molecular epidemiology of the novel coronavirus that causes severe acute respiratory syndrome. *Lancet* **363:** 99-104.

3 Ksiazek, T.G., Erdman, D., Goldsmith, C.S., Zaki, S.R., Peret, T., Emery, S., Tong, S., Urbani, C., Comer, J.A., Lim, W., Rollin, P.E., Dowell, S.F., Ling, A.E., Humphrey, C.D., Shieh, W.J., Guarner, J., Paddock, C.D., Rota, P., Fields, B., Derisi, J., Yang, J.Y., Cox, N., Hughes, J.M., Leduc, J.W., Bellini, W.J., Anderson, L.J., Group, S.W. (2003) A novel coronavirus associated with severe acute respiratory syndrome. *N Engl J Med* **348:** 1953-66.

4 Lee, N., Hui, D., Wu, A., Chan, P., Cameron, P., Joynt, G.M., Ahuja, A., Yung, M.Y., Leung, C.B., To, K.F., Lui, S.F., Szeto, C.C., Chung, S., Sung,

J.J. (2003) A major outbreak of severe acute respiratory syndrome in Hong Kong. *N Engl J Med* **348:** 1986-94.

5 Peiris, J.S., Lai, S.T., Poon, L.L., Guan, Y., Yam, L.Y., Lim, W., Nicholls, J., Yee, W.K., Yan, W.W., Cheung, M.T., Cheng, V.C., Chan, K.H., Tsang, D.N., Yung, R.W., Ng, T.K., Yuen, K.Y., Group, S.S. (2003) Coronavirus as a possible cause of severe acute respiratory syndrome. *Lancet* **361:** 1319-25.

6 Zhong, N.S., Zheng, B.J., Li, Y.M., Poon, Xie, Z.H., Chan, K.H., Li, P.H., Tan, S.Y., Chang, Q., Xie, J.P., Liu, X.Q., Xu, J., Li, D.X., Yuen, K.Y., Peiris, Guan, Y. (2003) Epidemiology and cause of severe acute respiratory syndrome (SARS) in Guangdong, People's Republic of China, in February, 2003. *Lancet* **362:** 1353-8.

7 Hijawi, B., Abdallat, M., Sayaydeh, A., Alqasrawi, S., Haddadin, A., Jaarour, N., Alsheikh, S., Alsanouri, T. (2013) Novel coronavirus infections in Jordan, April 2012: epidemiological findings from a retrospective investigation. *East Mediterr Health J* **19 Suppl 1:** S12-8.

8 Korea Centers for Disease, C., Prevention (2015) Middle East Respiratory Syndrome Coronavirus Outbreak in the Republic of Korea, 2015. *Osong*

Public Health Res Perspect **6:** 269-78.

9 Zaki, A.M., Van Boheemen, S., Bestebroer, T.M., Osterhaus, A.D., Fouchier, R.A. (2012) Isolation of a novel coronavirus from a man with pneumonia in Saudi Arabia. *N Engl J Med* **367:** 1814-20.

10 Jeffers, S.A., Tusell, S.M., Gillim-Ross, L., Hemmila, E.M., Achenbach, J.E., Babcock, G.J., Thomas, W.D., Jr., Thackray, L.B., Young, M.D., Mason, R.J., Ambrosino, D.M., Wentworth, D.E., Demartini, J.C., Holmes, K.V. (2004) CD209L (L-SIGN) is a receptor for severe acute respiratory syndrome coronavirus. *Proc Natl Acad Sci U S A* **101:** 15748-53.

11 Li, F., Li, W., Farzan, M., Harrison, S.C. (2005) Structure of SARS coronavirus spike receptor-binding domain complexed with receptor. *Science* **309:** 1864-8.

12 Li, W., Moore, M.J., Vasilieva, N., Sui, J., Wong, S.K., Berne, M.A., Somasundaran, M., Sullivan, J.L., Luzuriaga, K., Greenough, T.C., Choe, H., Farzan, M. (2003) Angiotensin-converting enzyme 2 is a functional receptor for the SARS coronavirus. *Nature* **426:** 450-4.

13 Gao, W., Tamin, A., Soloff, A., D'aiuto, L., Nwanegbo, E., Robbins, P.D., Bellini, W.J., Barratt-Boyes, S., Gambotto, A. (2003) Effects of a

SARS-associated coronavirus vaccine in monkeys. *Lancet* **362:** 1895-6.

14 Hofmann, H., Hattermann, K., Marzi, A., Gramberg, T., Geier, M., Krumbiegel, M., Kuate, S., Uberla, K., Niedrig, M., Pohlmann, S. (2004) S protein of severe acute respiratory syndrome-associated coronavirus mediates entry into hepatoma cell lines and is targeted by neutralizing antibodies in infected patients. *J Virol* **78:** 6134-42.

15 Simmons, G., Reeves, J.D., Rennekamp, A.J., Amberg, S.M., Piefer, A.J., Bates, P. (2004) Characterization of severe acute respiratory syndrome-associated coronavirus (SARS-CoV) spike glycoprotein-mediated viral entry. *Proc Natl Acad Sci U S A* **101:** 4240-5.

16 Sui, J., Li, W., Murakami, A., Tamin, A., Matthews, L.J., Wong, S.K., Moore, M.J., Tallarico, A.S., Olurinde, M., Choe, H., Anderson, L.J., Bellini, W.J., Farzan, M., Marasco, W.A. (2004) Potent neutralization of severe acute respiratory syndrome (SARS) coronavirus by a human mAb to S1 protein that blocks receptor association. *Proc Natl Acad Sci U S A* **101:** 2536-41.

17 Wong, S.K., Li, W., Moore, M.J., Choe, H., Farzan, M. (2004) A 193-amino acid fragment of the SARS coronavirus S protein efficiently binds

angiotensin-converting enzyme 2. *J Biol Chem* **279:** 3197-201.

18 Zeng, F., Chow, K.Y., Hon, C.C., Law, K.M., Yip, C.W., Chan, K.H., Peiris, J.S., Leung, F.C. (2004) Characterization of humoral responses in mice immunized with plasmid DNAs encoding SARS-CoV spike gene fragments. *Biochem Biophys Res Commun* **315:** 1134-9.

19 Bisht, H., Roberts, A., Vogel, L., Bukreyev, A., Collins, P.L., Murphy, B.R., Subbarao, K., Moss, B. (2004) Severe acute respiratory syndrome coronavirus spike protein expressed by attenuated vaccinia virus protectively immunizes mice. *Proc Natl Acad Sci U S A* **101:** 6641-6.

20 Bukreyev, A., Lamirande, E.W., Buchholz, U.J., Vogel, L.N., Elkins, W.R., St Claire, M., Murphy, B.R., Subbarao, K., Collins, P.L. (2004) Mucosal immunisation of African green monkeys (Cercopithecus aethiops) with an attenuated parainfluenza virus expressing the SARS coronavirus spike protein for the prevention of SARS. *Lancet* **363:** 2122-7.

21 Chen, Z., Zhang, L., Qin, C., Ba, L., Yi, C.E., Zhang, F., Wei, Q., He, T., Yu, W., Yu, J., Gao, H., Tu, X., Gettie, A., Farzan, M., Yuen, K.Y., Ho, D.D. (2005) Recombinant modified vaccinia virus Ankara expressing the spike glycoprotein of severe acute respiratory syndrome coronavirus induces

protective neutralizing antibodies primarily targeting the receptor binding region. *J Virol* **79:** 2678-88.

22 He, Y., Li, J., Heck, S., Lustigman, S., Jiang, S. (2006) Antigenic and immunogenic characterization of recombinant baculovirus-expressed severe acute respiratory syndrome coronavirus spike protein: implication for vaccine design. *J Virol* **80:** 5757-67.

23 He, Y., Zhou, Y., Wu, H., Luo, B., Chen, J., Li, W., Jiang, S. (2004) Identification of immunodominant sites on the spike protein of severe acute respiratory syndrome (SARS) coronavirus: implication for developing SARS diagnostics and vaccines. *J Immunol* **173:** 4050-7.

24 Huang, J., Cao, Y., Du, J., Bu, X., Ma, R., Wu, C. (2007) Priming with SARS CoV S DNA and boosting with SARS CoV S epitopes specific for CD4+ and CD8+ T cells promote cellular immune responses. *Vaccine* **25:** 6981-91.

25 Yang, Z.Y., Kong, W.P., Huang, Y., Roberts, A., Murphy, B.R., Subbarao, K., Nabel, G.J. (2004) A DNA vaccine induces SARS coronavirus neutralization and protective immunity in mice. *Nature* **428:** 561-4.

26 Zhou, Z., Post, P., Chubet, R., Holtz, K., Mcpherson, C., Petric, M., Cox,

M. (2006) A recombinant baculovirus-expressed S glycoprotein vaccine elicits high titers of SARS-associated coronavirus (SARS-CoV) neutralizing antibodies in mice. *Vaccine* **24:** 3624-31.

27 Bolles, M., Deming, D., Long, K., Agnihothram, S., Whitmore, A., Ferris, M., Funkhouser, W., Gralinski, L., Totura, A., Heise, M., Baric, R.S. (2011) A double-inactivated severe acute respiratory syndrome coronavirus vaccine provides incomplete protection in mice and induces increased eosinophilic proinflammatory pulmonary response upon challenge. *J Virol* **85:** 12201-15.

28 Honda-Okubo, Y., Barnard, D., Ong, C.H., Peng, B.H., Tseng, C.T., Petrovsky, N. (2015) Severe acute respiratory syndrome-associated coronavirus vaccines formulated with delta inulin adjuvants provide enhanced protection while ameliorating lung eosinophilic immunopathology. *J Virol* **89:** 2995-3007.

29 Tseng, C.T., Sbrana, E., Iwata-Yoshikawa, N., Newman, P.C., Garron, T., Atmar, R.L., Peters, C.J., Couch, R.B. (2012) Immunization with SARS coronavirus vaccines leads to pulmonary immunopathology on challenge with the SARS virus. *PLoS One* **7:** e35421.

30 Kim, H.W., Canchola, J.G., Brandt, C.D., Pyles, G., Chanock, R.M., Jensen, K., Parrott, R.H. (1969) Respiratory syncytial virus disease in infants despite prior administration of antigenic inactivated vaccine. *Am J Epidemiol* **89:** 422-34.

31 Olson, M.R., Varga, S.M. (2008) Pulmonary immunity and immunopathology: lessons from respiratory syncytial virus. *Expert Rev Vaccines* **7:** 1239-55.

32 Openshaw, P.J., Culley, F.J., Olszewska, W. (2001) Immunopathogenesis of vaccine-enhanced RSV disease. *Vaccine* **20 Suppl 1:** S27-31.

33 Delgado, M.F., Coviello, S., Monsalvo, A.C., Melendi, G.A., Hernandez, J.Z., Batalle, J.P., Diaz, L., Trento, A., Chang, H.Y., Mitzner, W., Ravetch, J., Melero, J.A., Irusta, P.M., Polack, F.P. (2009) Lack of antibody affinity maturation due to poor Toll-like receptor stimulation leads to enhanced respiratory syncytial virus disease. *Nat Med* **15:** 34-41.

34 Iwata-Yoshikawa, N., Uda, A., Suzuki, T., Tsunetsugu-Yokota, Y., Sato, Y., Morikawa, S., Tashiro, M., Sata, T., Hasegawa, H., Nagata, N. (2014) Effects of Toll-like receptor stimulation on eosinophilic infiltration in lungs of BALB/c mice immunized with UV-inactivated severe acute respiratory

syndrome-related coronavirus vaccine. *J Virol* **88:** 8597-614.

35 Nagata, N., Iwata, N., Hasegawa, H., Fukushi, S., Harashima, A., Sato, Y., Saijo, M., Taguchi, F., Morikawa, S., Sata, T. (2008) Mouse-passaged severe acute respiratory syndrome-associated coronavirus leads to lethal pulmonary edema and diffuse alveolar damage in adult but not young mice. *Am J Pathol* **172:** 1625-37.

36 Ahmad, S., Zamry, A.A., Tan, H.T., Wong, K.K., Lim, J., Mohamud, R. (2017) Targeting dendritic cells through gold nanoparticles: A review on the cellular uptake and subsequent immunological properties. *Mol Immunol* **91:** 123-33.

37 Pati, R., Shevtsov, M., Sonawane, A. (2018) Nanoparticle Vaccines Against Infectious Diseases. *Front Immunol* **9:** 2224.

38 Zhao, L., Seth, A., Wibowo, N., Zhao, C.X., Mitter, N., Yu, C., Middelberg, A.P. (2014) Nanoparticle vaccines. *Vaccine* **32:** 327-37.

39 Niikura, K., Matsunaga, T., Suzuki, T., Kobayashi, S., Yamaguchi, H., Orba, Y., Kawaguchi, A., Hasegawa, H., Kajino, K., Ninomiya, T., Ijiro, K., Sawa, H. (2013) Gold nanoparticles as a vaccine platform: influence of size and shape on immunological responses in vitro and in vivo. *ACS Nano* **7:**

3926-38.

40 Dykman, L.A., Khlebtsov, N.G. (2017) Immunological properties of gold nanoparticles. *Chem Sci* **8:** 1719-35.

41 Fukushi, S., Fukuma, A., Kurosu, T., Watanabe, S., Shimojima, M., Shirato, K., Iwata-Yoshikawa, N., Nagata, N., Ohnishi, K., Ato, M., Melaku, S.K., Sentsui, H., Saijo, M. (2018) Characterization of novel monoclonal antibodies against the MERS-coronavirus spike protein and their application in species-independent antibody detection by competitive ELISA. *J Virol Methods* **251:** 22-29.

42 Matsuura, Y., Possee, R.D., Overton, H.A., Bishop, D.H. (1987) Baculovirus expression vectors: the requirements for high level expression of proteins, including glycoproteins. *J Gen Virol* **68 (Pt 5):** 1233-50.

43 Singh, H., Shimojima, M., Fukushi, S., Fukuma, A., Tani, H., Yoshikawa, T., Taniguchi, S., Yang, M., Sugamata, M., Morikawa, S., Saijo, M. (2016) Serologic assays for the detection and strain identification of Pteropine orthoreovirus. *Emerg Microbes Infect* **5:** e44.

44 Fukuma, A., Tani, H., Taniguchi, S., Shimojima, M., Saijo, M., Fukushi, S. (2015) Inability of rat DPP4 to allow MERS-CoV infection revealed by

using a VSV pseudotype bearing truncated MERS-CoV spike protein. *Arch Virol* **160:** 2293-300.

45 Reinhard, B.M., Sheikholeslami, S., Mastroianni, A., Alivisatos, A.P., Liphardt, J. (2007) Use of plasmon coupling to reveal the dynamics of DNA bending and cleavage by single EcoRV restriction enzymes. *Proc Natl Acad Sci U S A* **104:** 2667-72.

46 Ichinohe, T., Watanabe, I., Ito, S., Fujii, H., Moriyama, M., Tamura, S., Takahashi, H., Sawa, H., Chiba, J., Kurata, T., Sata, T., Hasegawa, H. (2005) Synthetic double-stranded RNA poly(I:C) combined with mucosal vaccine protects against influenza virus infection. *J Virol* **79:** 2910-9.

47 Li, F., Berardi, M., Li, W., Farzan, M., Dormitzer, P.R., Harrison, S.C. (2006) Conformational states of the severe acute respiratory syndrome coronavirus spike protein ectodomain. *J Virol* **80:** 6794-800.

48 Fields, B.N., Knipe, D.M., Howley, P.M. (2013) Fields virology, 6th edn. Philadelphia: Wolters Kluwer Health/Lippincott Williams & Wilkins.

49 Agnihothram, S., Yount, B.L., Jr., Donaldson, E.F., Huynh, J., Menachery, V.D., Gralinski, L.E., Graham, R.L., Becker, M.M., Tomar, S., Scobey, T.D., Osswald, H.L., Whitmore, A., Gopal, R., Ghosh, A.K., Mesecar, A.,

Zambon, M., Heise, M., Denison, M.R., Baric, R.S. (2014) A mouse model for Betacoronavirus subgroup 2c using a bat coronavirus strain HKU5 variant. *MBio* **5:** e00047-14.

50 Du, L., Zhao, G., He, Y., Guo, Y., Zheng, B.J., Jiang, S., Zhou, Y. (2007) Receptor-binding domain of SARS-CoV spike protein induces long-term protective immunity in an animal model. *Vaccine* **25:** 2832-8.

51 Faber, M., Lamirande, E.W., Roberts, A., Rice, A.B., Koprowski, H., Dietzschold, B., Schnell, M.J. (2005) A single immunization with a rhabdovirus-based vector expressing severe acute respiratory syndrome coronavirus (SARS-CoV) S protein results in the production of high levels of SARS-CoV-neutralizing antibodies. *J Gen Virol* **86:** 1435-40.

52 He, Y., Lu, H., Siddiqui, P., Zhou, Y., Jiang, S. (2005) Receptor-binding domain of severe acute respiratory syndrome coronavirus spike protein contains multiple conformation-dependent epitopes that induce highly potent neutralizing antibodies. *J Immunol* **174:** 4908-15.

53 See, R.H., Zakhartchouk, A.N., Petric, M., Lawrence, D.J., Mok, C.P., Hogan, R.J., Rowe, T., Zitzow, L.A., Karunakaran, K.P., Hitt, M.M., Graham, F.L., Prevec, L., Mahony, J.B., Sharon, C., Auperin, T.C., Rini,

J.M., Tingle, A.J., Scheifele, D.W., Skowronski, D.M., Patrick, D.M., Voss, T.G., Babiuk, L.A., Gauldie, J., Roper, R.L., Brunham, R.C., Finlay, B.B. (2006) Comparative evaluation of two severe acute respiratory syndrome (SARS) vaccine candidates in mice challenged with SARS coronavirus. *J Gen Virol* **87:** 641-50.

54 Woo, P.C., Lau, S.K., Tsoi, H.W., Chen, Z.W., Wong, B.H., Zhang, L., Chan, J.K., Wong, L.P., He, W., Ma, C., Chan, K.H., Ho, D.D., Yuen, K.Y. (2005) SARS coronavirus spike polypeptide DNA vaccine priming with recombinant spike polypeptide from Escherichia coli as booster induces high titer of neutralizing antibody against SARS coronavirus. *Vaccine* **23:** 4959-68.

55 Zhao, J., Li, K., Wohlford-Lenane, C., Agnihothram, S.S., Fett, C., Zhao, J., Gale, M.J., Jr., Baric, R.S., Enjuanes, L., Gallagher, T., Mccray, P.B., Jr., Perlman, S. (2014) Rapid generation of a mouse model for Middle East respiratory syndrome. *Proc Natl Acad Sci U S A* **111:** 4970-5.

56 Song, Z., Xu, Y., Bao, L., Zhang, L., Yu, P., Qu, Y., Zhu, H., Zhao, W., Han, Y., Qin, C. (2019) From SARS to MERS, Thrusting Coronaviruses into the Spotlight. *Viruses* **11**.

57 Agrawal, A.S., Tao, X., Algaissi, A., Garron, T., Narayanan, K., Peng, B.H., Couch, R.B., Tseng, C.T. (2016) Immunization with inactivated Middle East Respiratory Syndrome coronavirus vaccine leads to lung immunopathology on challenge with live virus. *Hum Vaccin Immunother* **12:** 2351-6.

58 Mukhopadhyay, A., Basu, S., Singha, S., Patra, H.K. (2018) Inner-View of Nanomaterial Incited Protein Conformational Changes: Insights into Designable Interaction. *Research (Wash D C)* **2018:** 9712832.

59 Nguyen, V.H., Lee, B.J. (2017) Protein corona: a new approach for nanomedicine design. *Int J Nanomedicine* **12:** 3137-51.

60 Monopoli, M.P., Aberg, C., Salvati, A., Dawson, K.A. (2012) Biomolecular coronas provide the biological identity of nanosized materials. *Nat Nanotechnol* **7:** 779-86.

61 Lacerda, S.H., Park, J.J., Meuse, C., Pristinski, D., Becker, M.L., Karim, A., Douglas, J.F. (2010) Interaction of gold nanoparticles with common human blood proteins. *ACS Nano* **4:** 365-79.

62 Russell, B.A., Jachimska, B., Komorek, P., Mulheran, P.A., Chen, Y. (2017) Lysozyme encapsulated gold nanoclusters: effects of cluster synthesis on

natural protein characteristics. *Phys Chem Chem Phys* **19:** 7228-35.

63 Levy, D.E., Marie, I.J., Durbin, J.E. (2011) Induction and function of type I and III interferon in response to viral infection. *Curr Opin Virol* **1:** 476-86.

64 Stetson, D.B., Medzhitov, R. (2006) Type I interferons in host defense. *Immunity* **25:** 373-81.

65 Nagata, N., Iwata, N., Hasegawa, H., Fukushi, S., Yokoyama, M., Harashima, A., Sato, Y., Saijo, M., Morikawa, S., Sata, T. (2007) Participation of both host and virus factors in induction of severe acute respiratory syndrome (SARS) in F344 rats infected with SARS coronavirus. *J Virol* **81:** 1848-57.

66 Chen, J., Lau, Y.F., Lamirande, E.W., Paddock, C.D., Bartlett, J.H., Zaki, S.R., Subbarao, K. (2010) Cellular immune responses to severe acute respiratory syndrome coronavirus (SARS-CoV) infection in senescent BALB/c mice: CD4+ T cells are important in control of SARS-CoV infection. *J Virol* **84:** 1289-301.

67 Page, C., Goicochea, L., Matthews, K., Zhang, Y., Klover, P., Holtzman, M.J., Hennighausen, L., Frieman, M. (2012) Induction of alternatively activated macrophages enhances pathogenesis during severe acute

respiratory syndrome coronavirus infection. *J Virol* **86:** 13334-49.

68 Tazaki, T., Tabata, K., Ainai, A., Ohara, Y., Kobayashi, S., Ninomiya, T., Orba, Y., Mitomo, H., Nakano, T., Hasegawa, H., Ijiro, K., Sawa, H., Suzuki, T., Niikura, K. (2018) Shape-dependent adjuvanticity of nanoparticleconjugated RNA adjuvants for intranasal inactivated influenza vaccines. *RSC advances* **8:** 16527-36.

69 Mottram, P.L., Leong, D., Crimeen-Irwin, B., Gloster, S., Xiang, S.D., Meanger, J., Ghildyal, R., Vardaxis, N., Plebanski, M. (2007) Type 1 and 2 immunity following vaccination is influenced by nanoparticle size: formulation of a model vaccine for respiratory syncytial virus. *Mol Pharm* **4:** 73-84.

70 Leenaars, M., Hendriksen, C.F. (2005) Critical steps in the production of polyclonal and monoclonal antibodies: evaluation and recommendations. *ILAR J* **46:** 269-79.

Figure 1. Preparation of recombinant SARS spike protein. (a) Schematic structure of the spike protein and the recombinant protein (Strep-8xHis-tagged at the C-terminus of the ectodomain). SP, signal peptide; RBD, receptor binding domain; TM, transmembrane domain. (b) Purified recombinant protein. CB, Coomassie blue staining; WB, western blot analysis of the recombinant proteins using anti-penta-His and anti-SARS-S antibodies. S-protein, purified recombinant protein; Pre, culture supernatant; Flow through, flow through fraction from the column.

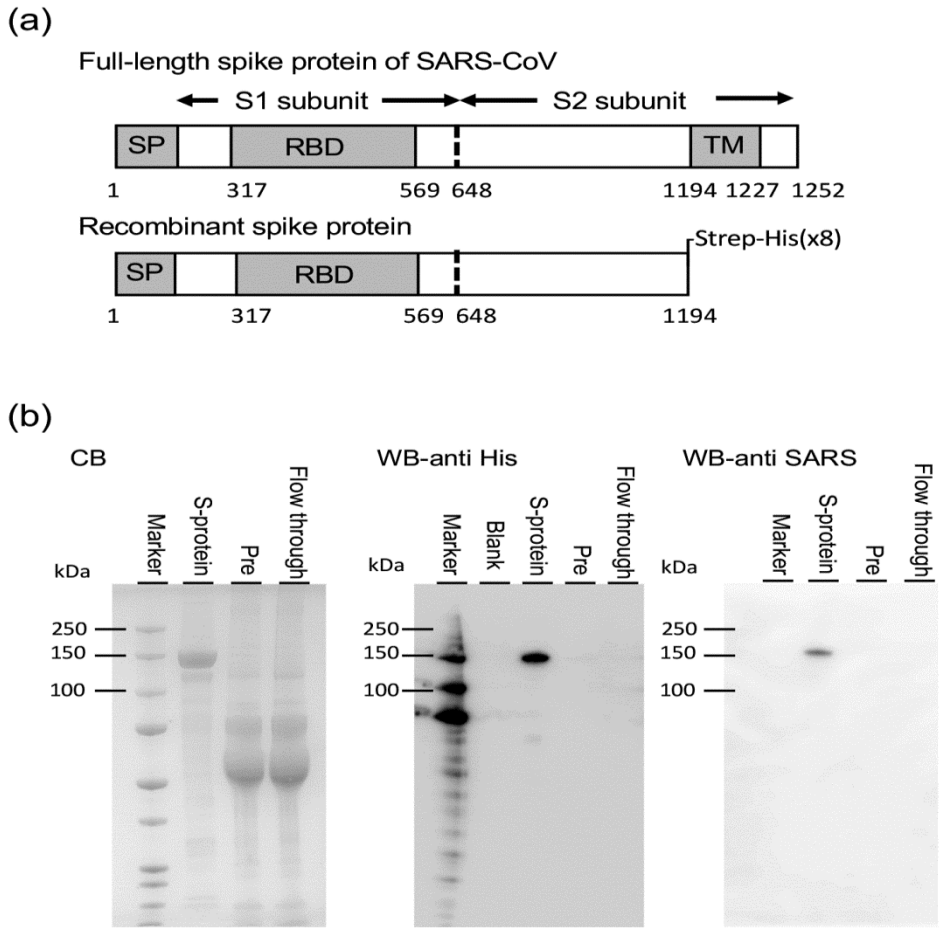

Figure 2. Immunogenicity of the recombinant SARS S protein in mice. Female BALB/c mice were subcutaneously immunized with the purified recombinant S protein at 1.0, 0.5, 0.1, or 0.05 μg/immunization (n = 6-7). After the second immunization, the mice were inoculated with 10^6 $TCID_{50}$ of mouse-adapted SARS-CoV. (a) Antigen-specific IgG titer in the sera 2 weeks after the second immunization. The detection limit was 1:10. Each dot shows the data from an individual animal. *, $p < 0.05$. Tukey's multiple comparisons test following by one-way ANOVA. (b) Body weight changes after SARS-CoV challenge infection. *, $p < 0.05$; **, $p < 0.01$; ***, $p < 0.001$; ****, $p < 0.0001$. Comparison of the body weight changes with those of the control group via Tukey's multiple comparisons test following one-way ANOVA. (c) Survival curves after SARS-CoV challenge. Comparisons of survival with respect to the control group were performed using the log-rank test following by Kaplan-Meier survival analysis.

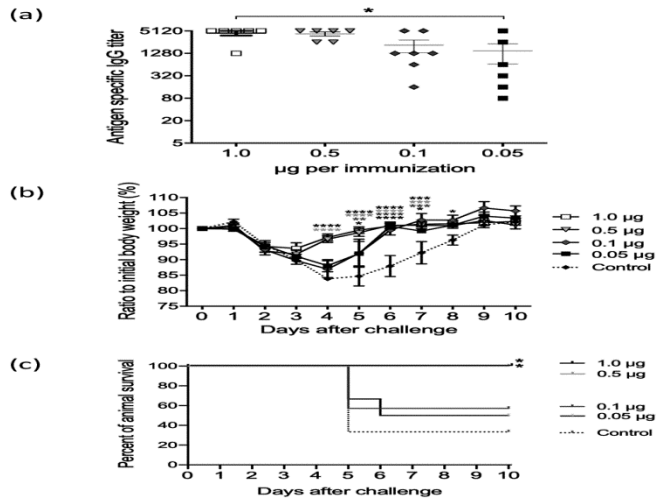

Figure 3. Lung histopathology in recombinant S protein-immunized mice on day 10 post-challenge. The lung tissue samples are from the same animals used in the experiment shown in Figure 2. (a) Representative histopathological findings of mice with the highest eosinophil infiltration detected by eosinophil staining using the C.E.M. kit. Eosinophil infiltrations occurred around middle size blood vessels in the bronchi area. The arrows indicate eosinophils. Br, bronchi; V, brood vessel; Control, PBS pre-treated challenge control on day 4 post-infection. Slight inflammatory cell infiltrations with a few mononuclear cells and eosinophils occurred around the blood vessels with edema. Upper panels, low magnification (bars, 100 μm); Lower panels, high magnification (bars, 20 μm). (b) Number of eosinophils per lung section (n = 6–7) on day 10 post-challenge. Five 147,000-μm^2 regions around the pulmonary bronchiole of each mouse were scored at 600× magnification. Each dot shows the data from an individual animal. The brown-colored symbols indicate data from moribund animals within 10 d.p.i. *, $p < 0.05$; **, $p < 0.01$, via Tukey's multiple comparisons test following by one-way ANOVA for comparisons with the control group.

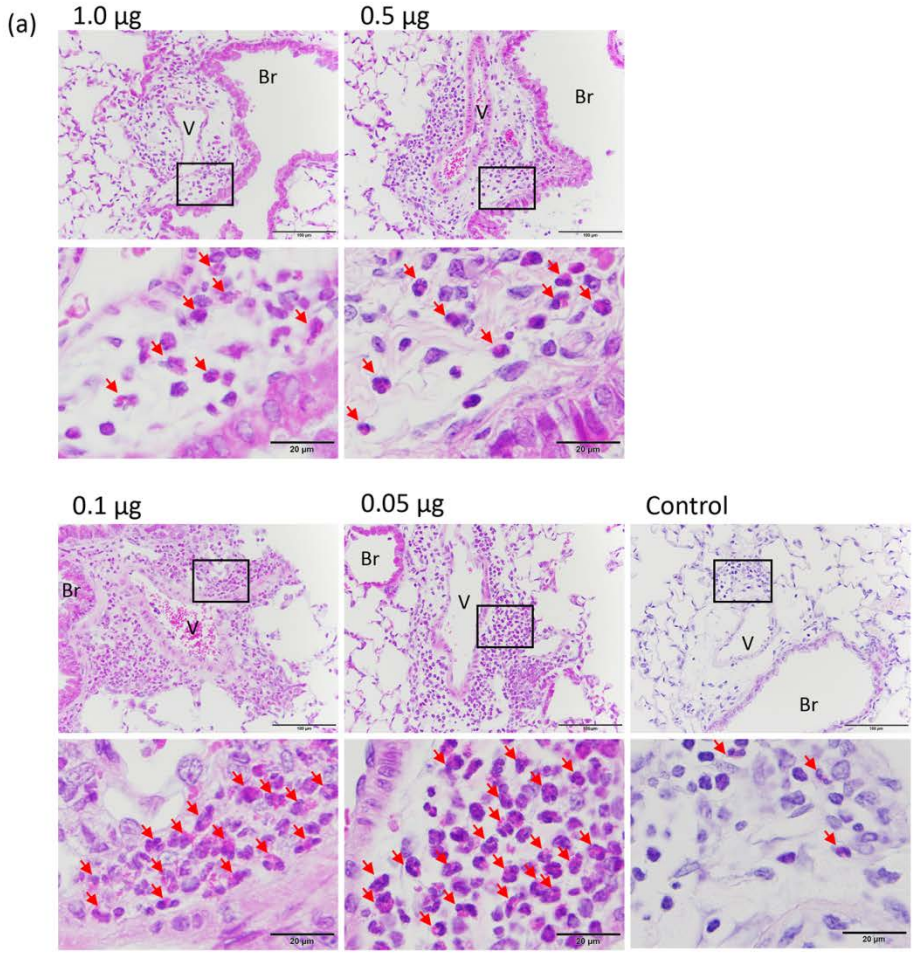

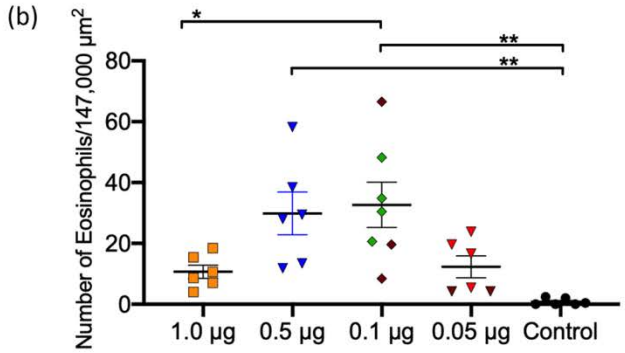

Figure 4. Quantification of the gold nanoparticle-protein complex (S+AuNPs). (a–c) Virus-specific IgG titer after the second immunization. 0.5 μg S protein in an AuNP solution containing 0.1 nM particles was diluted and used for immunization (a). 0.5 μg, 0.1 μg, or 0.05 μg S protein with 10 fmol AuNPs was used for immunization (b). 0.1 μg S protein with 2 fmol of 40- or 100-nm AuNPs was used for immunization (c). The dash line indicates the limit of detection (<10). Each dot shows the data from an individual animal. *, $p < 0.05$. Dunn's multiple comparison test. (d) Western blot analysis of the samples during the preparation of S+AuNPs. S protein, 50 ng of purified S protein; Sup1, supernatant from S+AuNP solution produced via centrifugation at 2000 *g* for 10 min, i.e., free S protein in S+AuNP solution; sup2, wash buffer supernatant from the S+AuNP pellet; Binding S, S protein bound to BSPP-AuNPs. (e) Transmission electron microscopy images of recombinant proteins (S protein), BSPP-treated gold nanoparticles (BSPP-AuNPs), and S protein-conjugated gold nanoparticles (S+AuNPs) (bars, 200 nm). Particles and free protein are present in the S+AuNPs solution. The arrows indicate S protein-bound AuNPs. Protein "corona" means layers of bound proteins around AuNPs (inset, bars 20 nm).

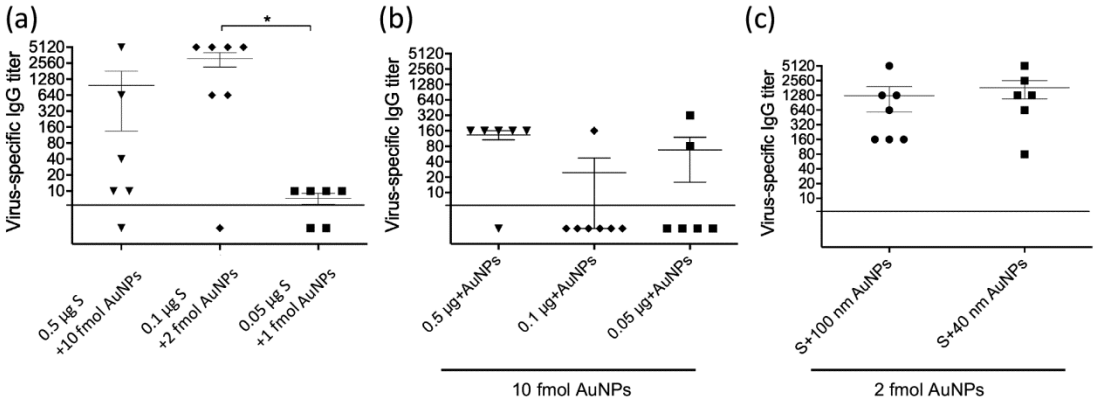

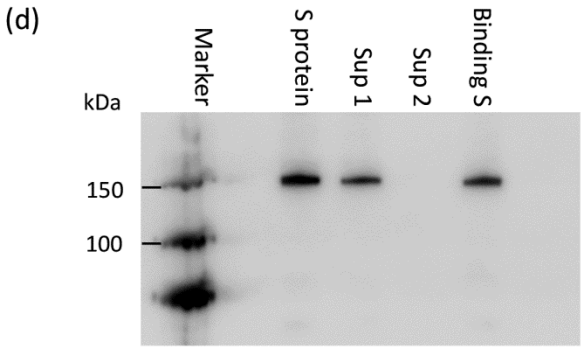

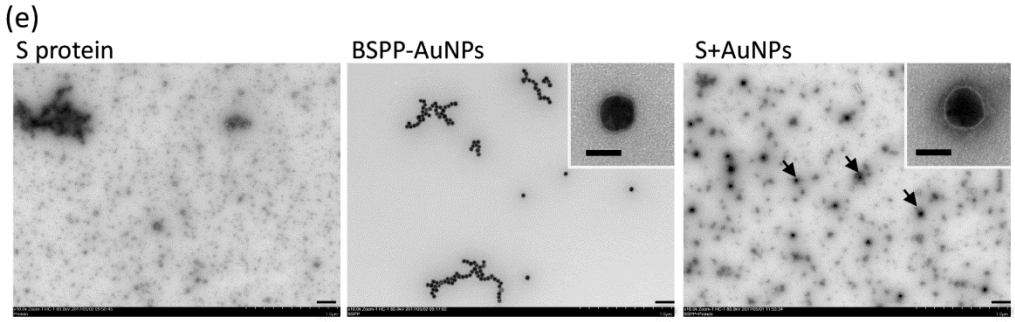

Figure 5. Effects of adjuvants on the outcomes of immunization with recombinant spike protein. Female BALB/c mice were vaccinated with each antigen. Mice immunized with 0.1 μg S protein with or without adjuvant were challenged with 10^6 $TCID_{50}$ of mouse-adapted SARS-CoV (n = 6-7). (a) Antigen-specific IgG titer in the sera 2 weeks after the second immunization. The line indicates the limit of detection (<10). Each dot shows the data from an individual animal. **, $p < 0.01$; ***, $p < 0.001$, via Dunn's multiple comparison test. (b) Virus-specific IgG titer after the second immunization. The dashed line indicates the limit of detection (<10). Each dot shows the data from an individual animal. *, $p < 0.05$; **, $p < 0.01$, via Dunn's multiple comparison test. (c) Serum neutralizing titers after the second immunization. The line indicates the limit of detection (<4). Each dot shows the data from an individual animal. *, $p < 0.05$; **, $p < 0.01$, via Dunn's multiple comparison test. (d) Body weight changes after SARS-CoV challenge infection. **, $p < 0.01$; ****, $p < 0.0001$. Tukey's multiple comparisons test following one-way ANOVA were used to compare the results with those of the control group. (e) Survival curves after SARS-CoV challenge infection. The log-rank test following Kaplan–Meier survival analysis was used to compare the survival with that of the control group. *, $p < 0.05$; **, $p < 0.01$.

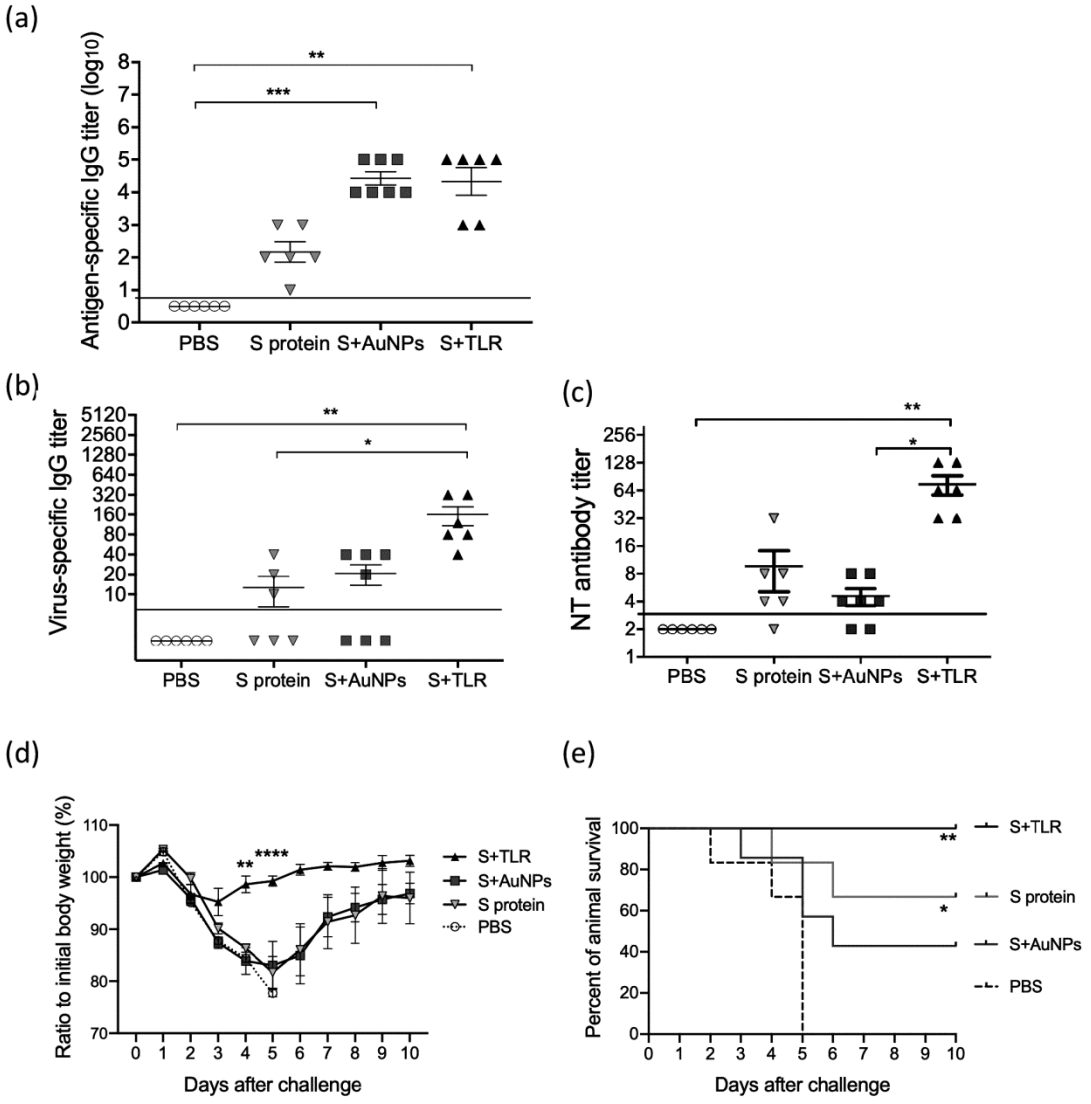

Figure 6. Lung histopathology from S protein-immunized mice with adjuvant on day 10 post-challenge. The lung tissue samples were from the same animals used in the experiment shown in Figure 5. (a) Representative histopathological findings from the mice with the highest eosinophil infiltration was detected via eosinophil staining using the C.E.M. kit. The red arrows indicate representative eosinophils, and the blue arrows indicate plasma cells. Br, bronchi; V, brood vessel. Results of the PBS, or AuNPs pre-treated controls on day 4 or 5 post-challenge infection. Upper panels, low magnification (bars, 100 μm); Lower panels, high magnification (bars, 20 μm). (b) Number of eosinophils per lung section (n = 6-7) on day 10 post-challenge. Five 147,000 μm^2 regions around the pulmonary bronchiole of each mouse were counted at 600× magnification. Each circle shows the mean value from an individual animal. Brown-colored symbols indicate data from moribund animals. *, $p < 0.05$; **, $p < 0.01$, via Tukey's multiple comparisons test following one-way ANOVA comparing the results with those of the control group.

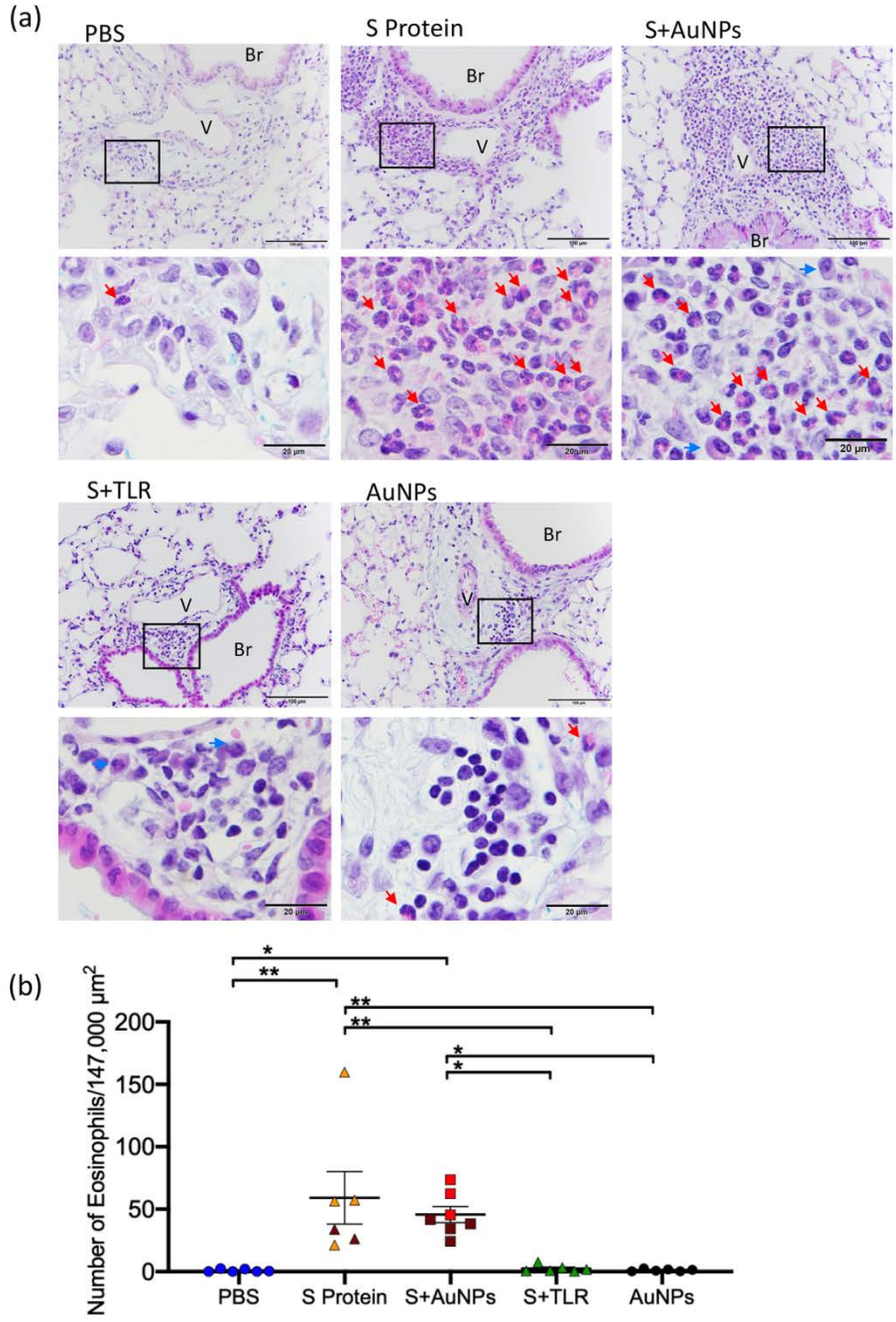

Figure 7. Protection against SARS-CoV challenge in mice immunized with adjuvanted SARS-CoV S protein. Samples from the lungs of immunized or non-immunized mice after SARS-CoV inoculation (n = 3-5). Virus titers (a) and mRNA expression levels of type 1 IFN in lungs 1, 3, and 5 days post-challenge (b). The assays were performed using unicate samples per animal. Each circle shows the data from an individual animal. * $p < 0.05$; **, $p < 0.01$; ***, $p < 0.001$; ****, $p < 0.0001$, via Tukey's multiple comparisons test following two-way ANOVA to compare the results with those of the control group.

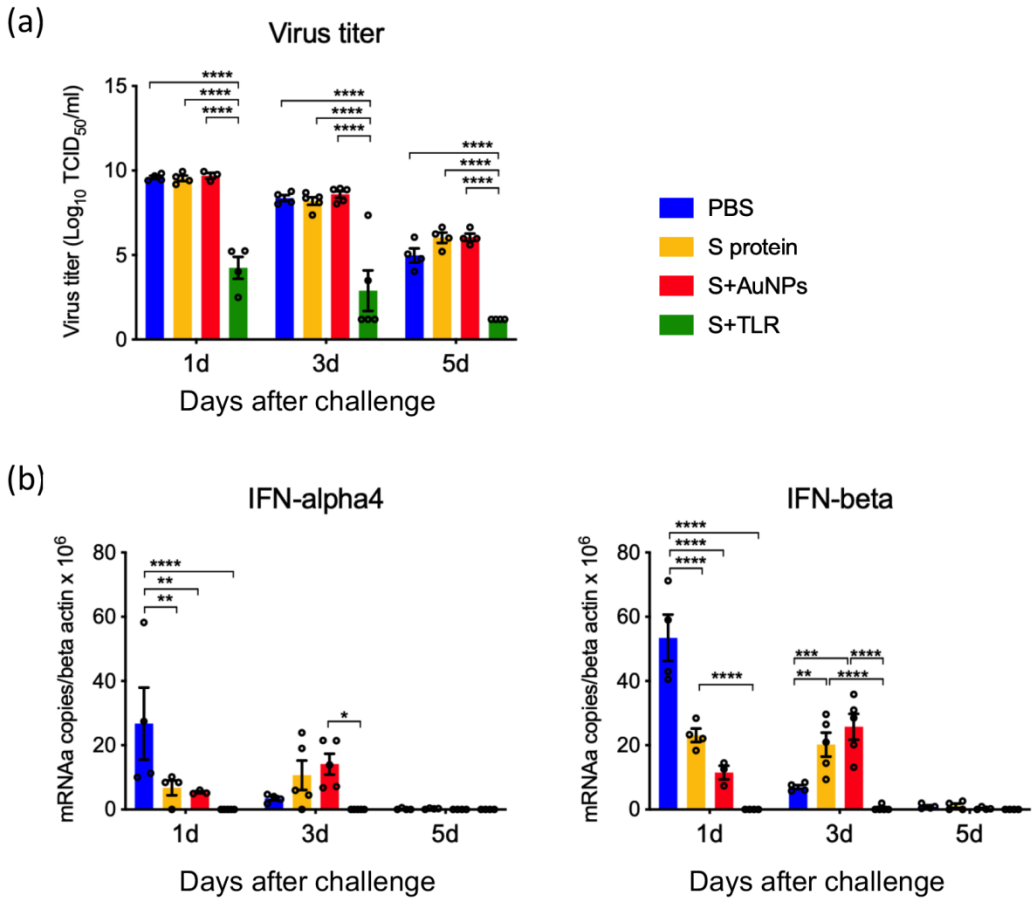

Figure 8. Immune responses in the lungs of mice immunized with adjuvant after SARS-CoV challenge. Cytokine and chemokine levels in the lungs of immunized or non-immunized animals 1, 3, and 5 days after infection with SARS-CoV (n = 3-5). The lung homogenates were from the same animals used in the experiment shown in Figure 7, and the assays were performed using unicate samples per animal. Each circle shows the data from an individual animal. * $p < 0.05$; **, $p < 0.01$; ***, $p < 0.001$; ****, $p < 0.0001$, via Tukey's multiple comparisons test following two-way ANOVA to compare the results with those of the control group.

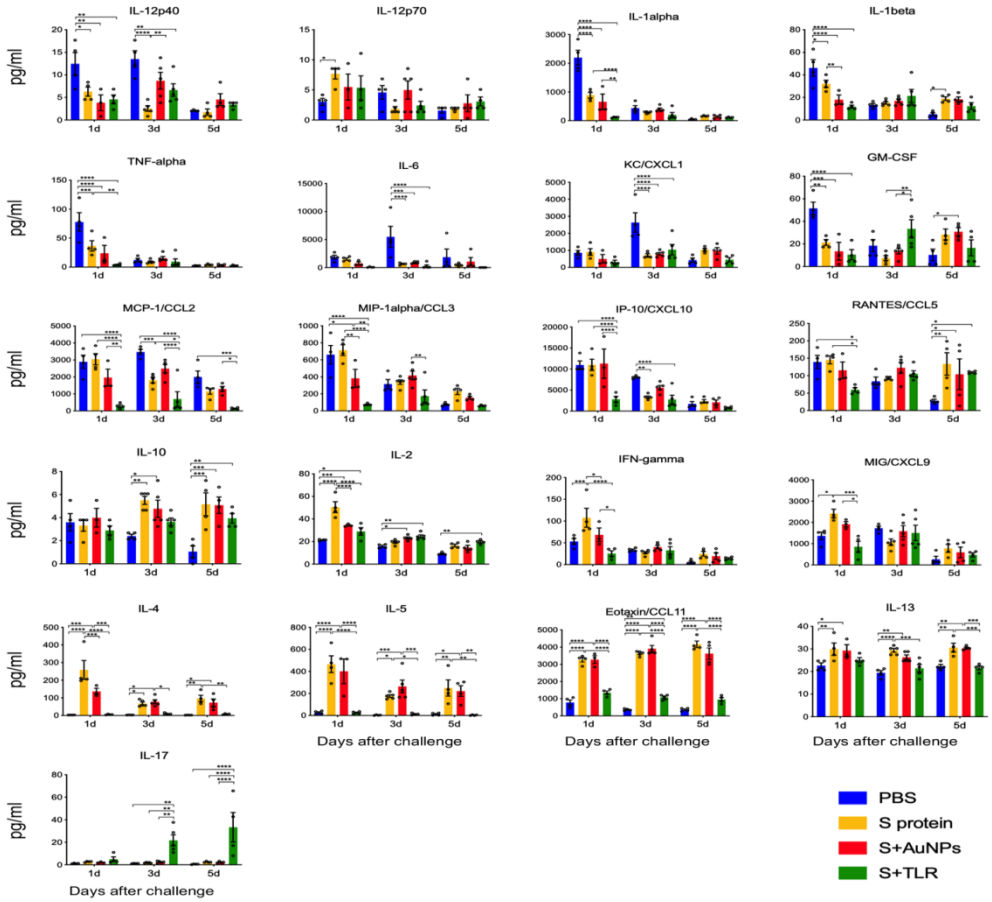

Table 1. Sizes of the AuNP-protein complex

	Diameter (nm) †		
AuNPs	Pre-treated	BSPP coated	S protein coated
40 nm	45.5 + 0.6	52.4 + 0.1	93.9 + 1.0
100 nm	107.2 + 0.1	121.9 + 0.3	173.3 + 2.4

† determined by dynamic light scattering (means + SEM of three independent measurements)